

Parametric study of filler size and properties for a liquid-metal thermal energy storage

Klarissa Niedermeier^{a,*}, Franziska Müller-Trefzer^a, Luca Marocco^b

^aKarlsruhe Institute of Technology (KIT), Institute for Thermal Energy Technology and Safety, Hermann-von-Helmholtz-Platz 1, 76344 Eggenstein-Leopoldshafen, Germany

^bPolitecnico di Milano, Department of Energy, via Lambruschini 4, 20156 Milan, Italy

Abstract

Liquid metals are promising heat transfer fluids since they remain liquid in a wide temperature range and can transfer heat efficiently due to their high thermal conductivity. A first-of-its-kind lab-scale thermal energy storage system with filler material and with lead-bismuth as heat transfer fluid is currently tested at the Karlsruhe Institute of Technology, while a 100-kWh storage system is under construction. This numerical study aims to analyse the influence of the filler parameters on the system's efficiency when the fluid used is a liquid metal. The filler should store part of the thermal energy, be efficiently discharged during the cyclic process and buffer the degradation of the thermocline during standby. For each of these purposes different particle diameters and values of some thermophysical properties of the filler, such as thermal conductivity, specific heat capacity and density, may be advantageous. Their influence on the thermocline extension is numerically investigated using a one-dimensional concentric dispersion model.

The results of the parameter study show that for an efficient discharge process in a liquid metal dual-media storage, a small filler particle size is beneficial ($d < 10$ mm for the reference case chosen in this work). In contrast, the standby phase is favored by larger diameters, here an order of 10–20 mm. Furthermore, a high thermal conductivity of the filler material improves the discharge performance, due to the enhanced heat transfer, but leads to an accelerated growth of the thermocline during standby. For this case, the optimum value is 5–10 W/mK. Moreover, using a filler material with a high volumetric heat capacity leads to the best overall performance.

A full factorial analysis shows that the filler diameter has the strongest effect on the discharge behaviour, while, during standby, the volumetric heat capacity has the largest influence.

Keywords: liquid metal, thermal energy storage, filler material, packed bed

1. Introduction

Thermal energy storage systems play an important role for a constant and reliable heat generation under fluctuating renewable energy generation. One example is the concentrating solar power technology, where large-scale thermal energy storage systems with molten salt already enable a 24/7 operation [1]. But also the implementation in conventional coal-fired or nuclear power plants is proposed with the aim of increasing the capacity factors and minimizing the number of start-ups [2, 3, 4].

Liquid metals as heat transfer fluids offer the advantage of excellent heat transfer characteristics and a broad operating temperature range [5, 6]. Sodium, for example, is liquid between 98 and 883 °C (1 bar) and the eutectic mixture of lead and bismuth (LBE) is liquid between 125 and 1533 °C (1 bar) [7, 8]. Therefore, they have been proposed as heat transfer fluids in concentrating solar power

plants [9, 10, 5, 11] and also for the use in thermal energy storage systems [12, 13, 14, 15].

A dual-media thermal energy storage system with filler material and liquid metal as heat transfer fluid is proposed by the authors as an efficient storage solution in previous publications, with the possibility to bring down the storage material costs as well [16, 17, 18].

At the Karlsruhe Institute of Technology (KIT), a dual-media thermal energy storage system with LBE has been demonstrated for the first time on a lab scale. Currently, a 100 kWh pilot-scale storage system is under construction.

For the proper design of its packed bed, some filler parameters are analysed in this study and general conclusions are derived about their impact on the efficiency of the liquid metal system. In a storage system with liquid metals, which have a very high thermal conductivity, the storage material must be chosen in such a way as to maintain sufficient stratification during the standby periods and at the same time ensure a good heat transfer during the charge and discharge phases. These opposing requirements for standby and cycling are discussed in this study.

In previous works [17, 19, 18] the influence of the tank

*Corresponding author

Email address: klarissa.niedermeier@kit.edu (Klarissa Niedermeier)

height, bed porosity, fluid velocity, particle diameter, fluid inlet temperature and initial storage temperature on the discharge and standby performance of a large-scale liquid-metal dual-media storage system was investigated by varying one factor at a time. The results indicate that large tank height-to-diameter ratios, a low porosity and small particle sizes are to be preferred.

Previous literature works for thermal storage systems with molten salts or oils, show that the discharge efficiency is independent of the thermal conductivity for small grain sizes of the filler material [20] while it increases with the thermal conductivity for larger grain sizes [21, 22, 23]. In fact, while for such fluids and for sufficiently small grain sizes the conductive thermal resistance of the material is negligible compared to the convective thermal resistance, this is not the case with liquid metals which practically always have a high Biot number [17]. Consequently, the lumped capacitance method, used in previous work with molten salts and oils [20, 22, 24, 25, 26], is not applicable here and it is necessary instead to solve the energy equation even in the solid phase, as discussed in [17, 18]. For an overview of numerical methods to simulate thermoclines, the interested reader is referred to Ref. [27].

To date, a parametric analysis of the key filler material properties that determine the efficiency of a liquid metal storage system, such as size, thermal conductivity, and volumetric heat capacity, is absent. This is done in the present work considering the configuration of the 100 kWh pilot plant currently under construction at KIT. In addition to the discharge phase alone, the combination of discharge and standby is also considered, the latter being particularly challenging for liquid metals as a result of their high thermal conductivity, which promotes thermocline degradation. The results were also analysed by full-factorial analysis to determine which of the parameters had the greatest impact on the efficiency and the mutual interactions between them. It should be noted that the compatibility between liquid metals and filler material, an important aspect due to the high corrosiveness of such fluids, is not considered in this study but will be experimentally analysed at the KIT.

2. Model description

A one-dimensional concentric dispersion model, discussed and validated in previous works by the same authors [17, 18], is used to simulate the discharge and standby process. Due to the high Biot number when using liquid metal as heat transfer fluids, the temperature profile inside the particles needs to be solved. The following assumptions are made:

- no axial heat conduction in the solid phase, as only point contact between the spherical filler particles
- no heat losses to the ambient, i.e. ideally insulated tank
- uniform fluid velocity and temperature across the cross section of the tank

- isotropic packed bed with monodisperse, spherical filler particles

2.1. Governing equation

The energy equation is solved for the fluid (Eq. 1) and the solid filler spheres (Eq. 2). The equations are coupled through a convective boundary condition at the surface of the filler spheres ($T_{p,o}$). For the standby process, the fluid velocity u is set to zero. Figure 1 shows a scheme of the simulated storage system.

$$\frac{\partial \varepsilon (\rho c_p)_f T}{\partial t} + \frac{\partial \varepsilon (\rho c_p)_f u T}{\partial x} = \frac{\partial}{\partial x} \left(\varepsilon \lambda_f \frac{\partial T}{\partial x} \right) - h_v (T - T_{p,o}) \quad (1)$$

$$(\rho c_p)_s \frac{\partial T_p}{\partial t} = \lambda_s \frac{1}{y^2} \frac{\partial}{\partial y} \left(y^2 \frac{\partial T_p}{\partial y} \right) \quad (2)$$

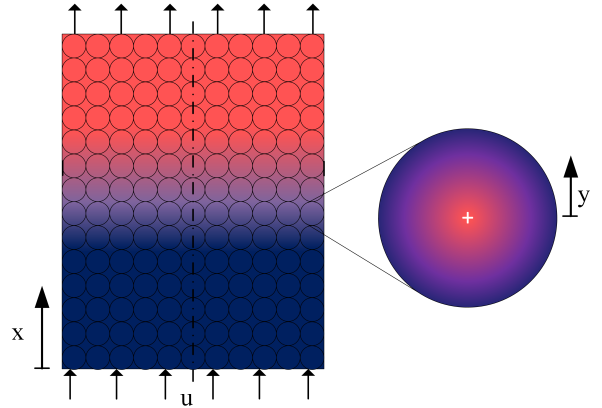


Figure 1: Scheme of a discharge process in a dual-media storage showing the temperature distribution in axial direction in the tank (x) and intra-particle radial direction (y), red: high temperature, blue: low temperature

2.2. Initial and boundary conditions

For the discharge process, the initial condition is of homogeneous temperature in the fluid and in the particles (T_{\max}), while for the standby simulation the initial temperatures for the fluid and the particles are those at the end of the discharge process, as shown in Eq. 3.

$$t = 0 : \begin{cases} T(x) = T_p(x, y) = T_{\max} & \text{discharge} \\ T(x) = T(x, t_{\text{dis}}) & \text{standby} \\ T_p(x, y) = T_p(x, y, t_{\text{dis}}) & \text{standby} \end{cases} \quad (3)$$

The boundary condition for the fluid is of constant temperature at the inlet and zero gradient at the outlet of the tank (Eq. 4-5). For standby, a zero gradient boundary condition is assumed at the inlet.

$$x = 0 : \begin{cases} T = T_{in} & \text{discharge} \\ \frac{\partial T}{\partial x} = 0 & \text{standby} \end{cases} \quad (4)$$

$$x = H : \quad \frac{\partial T}{\partial x} = 0 \quad \text{discharge/standby} \quad (5)$$

The filler spheres have a symmetry boundary condition in the centre and a convective boundary condition at the interface with the fluid (Eq. 6–7).

$$y = 0 : \quad \frac{\partial T_p}{\partial y} = 0 \quad (6)$$

$$y = d/2 : \quad -\lambda_s \frac{\partial T_p}{\partial y} = h_v(T - T_p) \quad (7)$$

2.3. Heat transfer between fluid and filler

The volumetric heat transfer coefficient h_v is calculated as the product of the (surface specific) heat transfer coefficient α and the specific surface of the particles s_v in the bed (Eq. 8).

$$h_v = \alpha \cdot s_v \quad \text{with} \quad \alpha = \frac{\text{Nu} \cdot \lambda_f}{d} \quad \text{and} \quad s_v = \frac{6(1 - \varepsilon)}{d} \quad (8)$$

Due to the lack of available literature correlations for the convective heat transfer coefficient between LBE and solid spheres in a packed bed [17], a conservative Nusselt number value of $\text{Nu} = 2$ was assumed.

2.4. Solution procedure

The energy conservation equations are solved with an in-house finite volume code. The time discretization is performed with a second-order Crank-Nicolson scheme. A central difference scheme is used for the spatial discretization of the diffusive terms, while a first order upwind scheme was chosen for the advective terms. The size of the control volumes in the filler particle is continuously reduced by a factor of 0.9 starting from the largest control volume in the center ($y = 0$).

A grid sensitivity analysis is performed according to Roache [28]. The number of control volumes is considered sufficient to provide the solution if the thermocline efficiency values obtained with two different grids differ by less than 0.2%. This implies, for the reference case, 1000 elements along the tank axis and 70 elements in the particles, considering a time step of 0.3 s for discharge and 3 s for standby.

3. Methodology

Firstly, a reference case is defined followed by the calculation of the storage and performance parameters and by an overview of the properties considered in the parameter study. Finally, the method of full factorial design of experiments is presented.

3.1. Reference case

The reference case and its operating temperature limits are based on the pilot-scale demonstrator that is currently under construction at KIT. The storage tank dimensions, mass flow, bed porosity and temperatures are defined as in the planned experiment:

- tank dimensions: $H = 2 \text{ m}$, $D = 0.6 \text{ m}$
- mass flow discharge: $\dot{m} = 2.43 \text{ kg s}^{-1}$
- $\vartheta_{\text{in}} = \vartheta_{x=0,t} = \vartheta_{\text{min}} = 200 \text{ }^\circ\text{C}$
- $\vartheta_{x,t=0} = \vartheta_{\text{max}} = 400 \text{ }^\circ\text{C}$
- bed porosity: $\varepsilon = 0.37$
- standby time: 480 min (8 h)

The storage tank size and the operating temperatures are limited by the space available for the test section of the liquid metal loop at KIT. In general, higher temperatures can be realized in liquid-metal storage systems.

The mass flow and the bed porosity are defined according to pre-tests in a lab-scale storage system at KIT. Thus, the numerical results can be used for the selection of a suitable filler material and, later on, to compare numerical and experimental results.

Table 1 lists the properties of LBE at $300 \text{ }^\circ\text{C}$, while in the simulation the temperature dependent properties from the LBE Handbook [8] are used.

Table 1: Physical properties of LBE (at $T = 300 \text{ }^\circ\text{C}$) [8]

$c_{pf}/\text{Jkg}^{-1}\text{K}^{-1}$	$\rho_f/\text{kg m}^{-3}$	$(\rho c_p)_f/\text{kJm}^{-3}\text{K}^{-1}$	$\lambda_f/\text{Wm}^{-1}\text{K}^{-1}$
146	10337	$1.5 \cdot 10^3$	12

3.2. Storage parameters

The storage capacity Q is determined from Eq. 9 with the properties taken at $T_{\text{mean}} = 0.5(T_{\text{max}} + T_{\text{min}})$.

$$Q = (m_f c_{pf} + m_s c_{ps})(T_{\text{max}} - T_{\text{min}}) \quad (9)$$

The fluid and solid mass (m_f and m_s) are evaluated with Eq. 10 and 11, respectively.

$$m_f = \varepsilon \frac{\pi D^2 H}{4} \rho_f \quad (10)$$

$$m_s = (1 - \varepsilon) \frac{\pi D^2 H}{4} \rho_s \quad (11)$$

3.3. Performance parameters of discharge and standby

Both discharge and standby are evaluated by determining the ratio of the thermocline zone, i.e. the zone x_{th} where the fluid temperature is between $\vartheta_{\text{min}} + 5 \text{ K}$ and $\vartheta_{\text{max}} - 5 \text{ K}$ (Fig. 2), and comparing it to the total tank height (Eq. 12).

$$\zeta = 1 - \frac{x_{\text{th}}}{H} \quad (12)$$

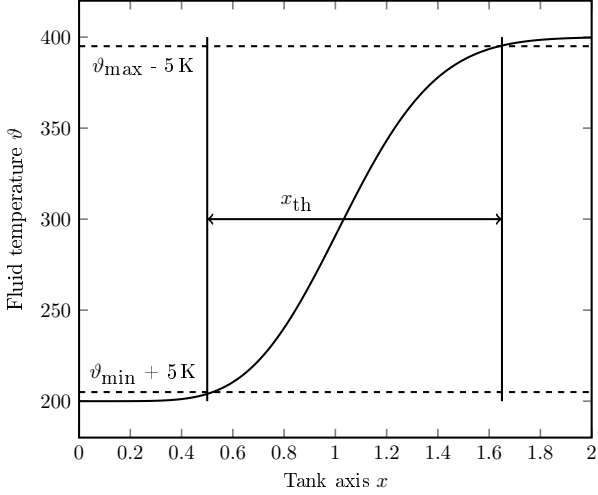


Figure 2: Example of a thermocline zone x_{th} as the part of the storage tank axis x (in m) with a fluid temperature ϑ (in °C) between $\vartheta_{min} + 5$ K and $\vartheta_{max} - 5$ K

An efficiency of $\zeta = 0$ represents the worst case, i.e. a storage tank filled completely with the thermocline region. An ideal storage system with a thermocline efficiency of $\zeta = 1$, by contrast, has an ideal separation of the hot and the cold zone.

The discharge process is simulated for half of the ideal discharge time starting from a fully charged tank (Eq. 13).

$$t_{dis} = \frac{1}{2} \cdot t_{dis,ideal} = \frac{1}{2} \cdot \frac{Q}{\dot{m}c_{pf}(T_{max} - T_{min})} \quad (13)$$

After this time interval, the thermocline zone x_{th} has moved to the centre of the tank. The next standby phase, simulated for 480 minutes (8 h), starts from the most unfavorable situation, being half of the tank at the minimum temperature and the other half at the maximum temperature.

The thermocline efficiency after half of the discharge time is defined as ζ_{dis} (Eq. 14) and after an additional standby of 480 min (8 h) as ζ_{st} (Eq. 15).

$$\zeta_{dis} = \zeta(t_{dis}) \quad (14)$$

$$\zeta_{st} = \zeta(t_{dis} + 480 \text{ min}) \quad (15)$$

The difference between the discharge efficiency ζ_{dis} and the total discharge and standby efficiency ζ_{st} represents the growth of the thermocline during standby (Eq. 16).

$$\Delta\zeta = \zeta_{st} - \zeta_{dis} \quad (16)$$

3.4. Parameter study

The base case for the parameter study is:

- filler diameter: $d = 50$ mm
- thermal conductivity: $\lambda_s = 5 \text{ Wm}^{-1}\text{K}^{-1}$
- volumetric heat capacity: $(\rho c_p)_s = 5 \cdot 10^3 \text{ kJm}^{-3}\text{K}^{-1}$

As the storage tank dimensions are kept constant, the storage capacity changes depending on the volumetric heat capacity $(\rho c_p)_s$ of the filler. Table 2 shows the variation ranges of the parameters and their influence on the storage capacity and efficiency.

The parameter range is chosen according to the review of Almendros-Ibáñez et al. [29] that list the typical thermal properties of filler material in packed-bed heat storage systems. The thermal conductivity of the filler is limited to the maximum value of 50 W/mK, since in order to minimize the degradation of the thermocline during standby, it must always be lower than the liquid metal's thermal conductivity.

Table 2: Overview of variation range of the parameters and their influence on the storage capacity and efficiency; \checkmark : has an influence, \times : has no influence

parameters	range	Q	ζ
d/mm	[1...100]	\times	\checkmark
$\lambda_s/\text{Wm}^{-1}\text{K}^{-1}$	[0.1...50]	\times	\checkmark
$(\rho c_p)_s/\text{kJm}^{-3}\text{K}^{-1}$	$[5 \cdot 10^2 \dots 5 \cdot 10^4]$	\checkmark	\checkmark

In Fig. 3 the reference case and the varied parameters are summarized.

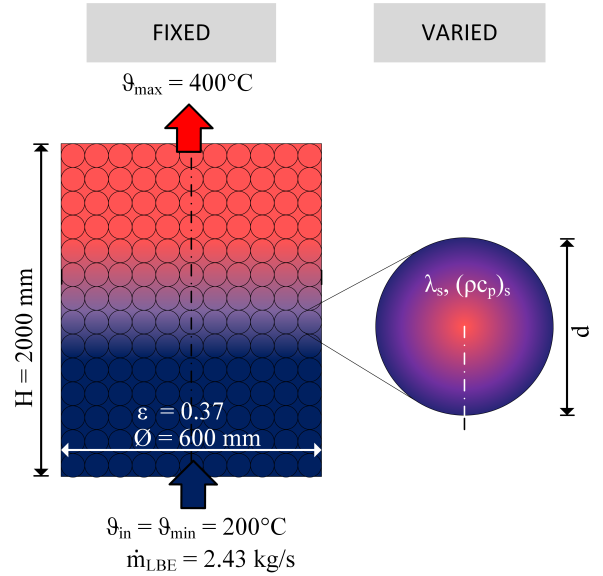


Figure 3: Scheme of the discharge process of a dual-media storage with the fixed and varied parameters in the parameter study

3.5. Analysis with full factorial design of experiments

In order to assess not only one factor at a time, but the combined effect of the three parameters varied in this study, additionally, an analysis with the method of full factorial design of experiments (DOE) is used [30]. It is used to determine the parameters with the largest effect on the results and their possible interactions.

This principle is schematically shown in Fig. 4. For $k = 3$ factors influencing a test result, a 2^k plan can be created with the test numbers representing the edges of the three-dimensional variation space of the three variables. The centre and the arrows represents the base case and the parameter study vectors, respectively.

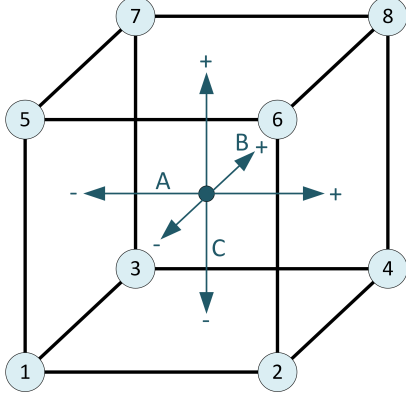


Figure 4: Schematic illustration of the three-dimensional parameter matrix according to the full factorial design of experiments, the numbers 1 to 8 representing the test numbers and A, B and C the influencing factors

In Table 3 the test plan with the $2^k - 1$ effects on the test result y_i is shown.

Table 3: Signs for the calculation of the effects and interactions of the three factors A, B and C

No.	A	B	C	AB	AC	BC	ABC	y_i
1	-	-	-	+	+	+	-	y_1
2	+	-	-	-	-	+	+	y_2
3	-	+	-	-	+	-	+	y_3
4	+	+	-	+	-	-	-	y_4
5	-	-	+	+	-	-	+	y_5
6	+	-	+	-	+	-	-	y_6
7	-	+	+	-	-	+	-	y_7
8	+	+	+	+	+	+	+	y_8
eff_j	eff_A	eff_B	eff_C	eff_{AB}	eff_{AC}	eff_{BC}	eff_{ABC}	

The effects are calculated with Eq. 17 [31].

$$\text{eff}_j = 1/4 \sum_{i=1}^8 (\text{sign} \cdot y_i) \quad (17)$$

The '+' sign stands for the maximum value of each factor A, B and C, the '-' sign the for the minimum value of each factor. The signs of the interactions are calculated as the products, e.g. $\text{sign}(AB) = \text{sign}(A) \cdot \text{sign}(B)$. The parameter ' y_i ' corresponds to the test result, i.e. is the thermocline efficiency ζ in this work. The calculation of the effect of the factor A (eff_A) on the test result is shown exemplarily in Eq. 18.

$$\text{eff}_A = 1/4 \cdot (-y_1 + y_2 - y_3 + y_4 - y_5 + y_6 - y_7 + y_8) \quad (18)$$

If the effect is negative it means that this factor has a reducing effect on the target value y ; a positive effect means that this factor is enhancing y . If the interaction effect, e.g. of AB, has the same sign as the effect of the main factor A, it implies that additionally increasing factor B has a boosting effect on the result y ; if it is the opposite sign it means it has a weakening effect [31].

4. Results

In the following, the simulation results for the reference case and the parameter study are shown. The discharge process is simulated starting from a fully charged tank for half of a discharge period and the standby for 480 min (8 h).

4.1. Reference case

Figure 5 presents the fluid temperature distribution along the vertical tank axis for four time steps during discharge. The thermal storage capacity of the reference case storage system (as described in Sec. 3.1) is 116.5 kWh with a total discharge time of $t_{\text{dis,ideal}} = 98$ min (1.64 h).

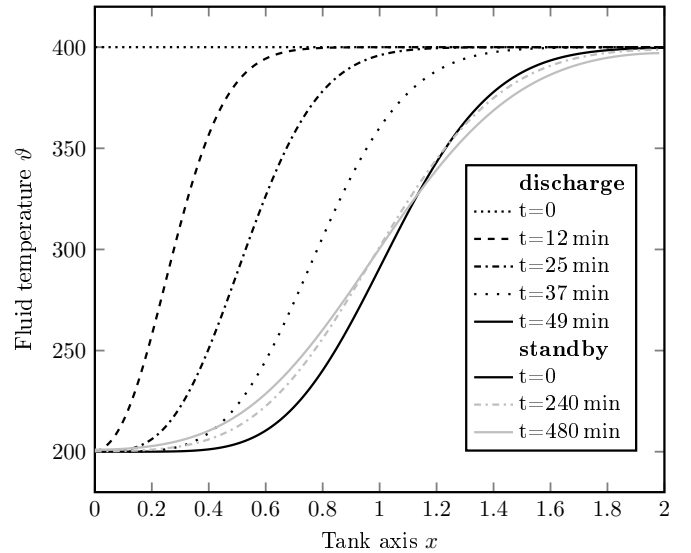


Figure 5: Fluid temperature ϑ (in $^{\circ}\text{C}$) distribution for the reference case along the vertical tank axis x (in m) at four time steps during discharge and during standby

It can be observed that during the discharge process, the thermocline moves through the tank and expands until the end of the simulated discharge process is reached (solid line, at 49 min). In gray, the temperatures during the following standby process are shown for 240 min (4 h) and 480 min (8 h).

Figure 6 shows the corresponding intra-particle temperature difference along the tank axis that decreases with time. This is the difference between the temperature in the centre of the particle ($T_{p,i}$) and its outer surface ($T_{p,o}$), i.e. $\Delta T_p = T_{p,i} - T_{p,o}$.

At the end of the discharge time t_{dis} the maximum value of the intra-particle temperature difference is $\Delta T_p \approx 10$ K

and reduces to values close to zero during standby due to the heat transfer to the surrounding LBE.

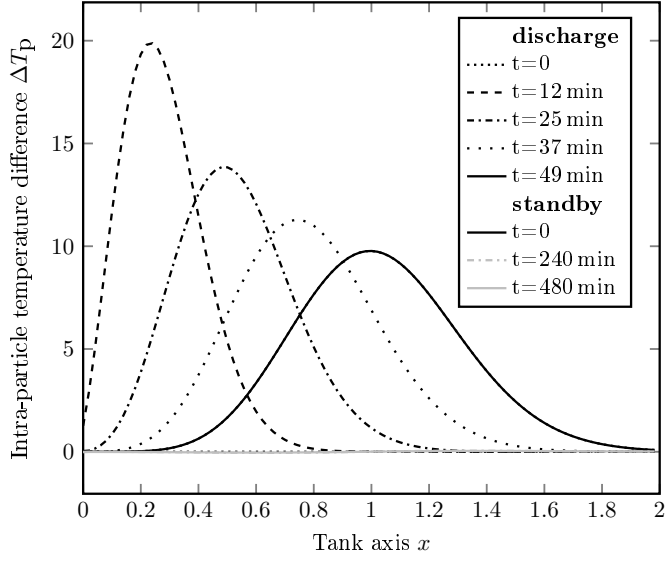


Figure 6: Intra-particle temperature difference ΔT_p (in K) for the reference case along the vertical tank axis x (in m) at four time steps during discharge and during standby

Figure 7 shows that the thermocline efficiency is 44.2% after discharge, i.e. 55.8% of the tank are filled with the thermocline zone. During the 480 min (8 h) of standby the efficiency decreases to 23.6%.

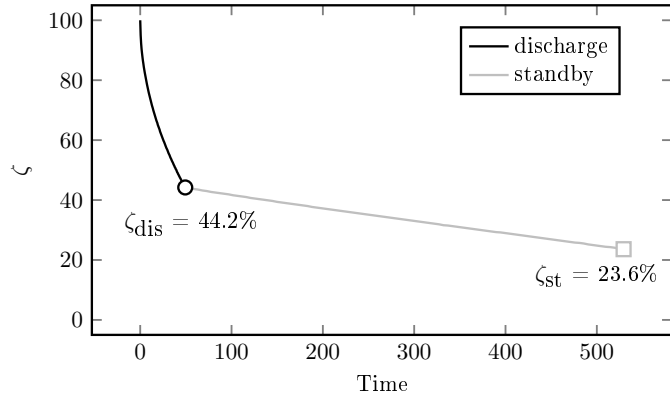


Figure 7: Thermocline efficiency ζ (in %) during 49 min of discharge and 480 min (8 h) standby for the reference case

4.2. Parameter study

In the following, the simulation results for different filler sizes and properties for both the discharge and standby phase are presented.

4.2.1. Variation of the filler particle diameter d

The fluid temperature and the intra-particle temperature difference are plotted in Fig. 8 and Fig. 9, where the solid line represents the base case results. By reducing the particle size, a reduced intra-particle temperature

difference is obtained during discharge, because the bigger surface-to-volume ratio implies a higher heat transfer from the filler material to the liquid metal. The maximum intra-particle temperature difference during discharge decreases from $\Delta T_{p,\max} = 20$ K ($d = 100$ mm) to $\Delta T_{p,\max} = 0.01$ K ($d = 1$ mm). This results in sharper fluid temperature profiles, with consequently reduced thermocline regions, and an improvement of the storage performance during discharge.

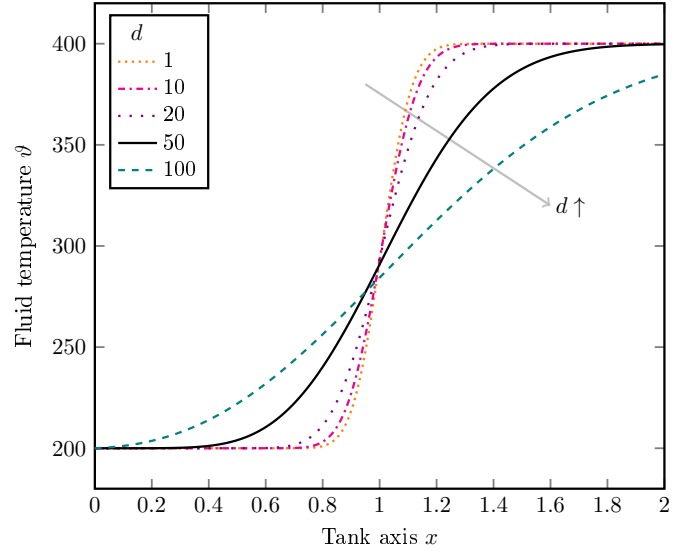


Figure 8: Fluid temperature θ (in °C) along the vertical tank axis x (in m) after discharge (t_{dis}) depending on the particle size d (in mm)

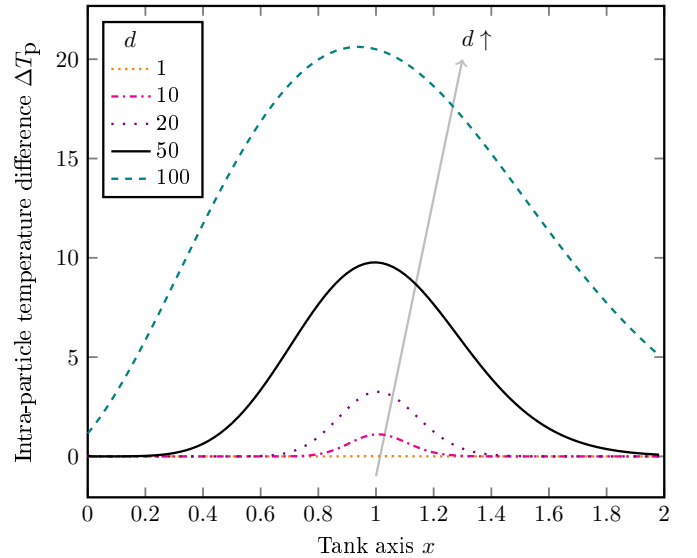


Figure 9: Intra-particle temperature difference ΔT_p (in K) along the vertical tank axis x (in m) after discharge (t_{dis}) depending on the particle size d (in mm)

Figure 10 shows that ζ_{dis} increases by reducing the particle diameter ($\zeta_{\text{dis}} = 11.9\%$ for $d = 100$ mm to $\zeta_{\text{dis}} = 83.6\%$ for $d = 1$ mm). For $d < 10$ mm the improvements by further decreasing the particle diameter are not significant, though.

The standby behaviour, by contrast, improves when choosing particles with a larger diameter, as the reduced heat transfer surface minimizes the heat transfer to the fluid, which is advantageous for the stratification in the tank. This can be observed by the decrease of the thermocline zone ($\Delta\zeta$) for increasing particle diameters.

For a standby time here considered, the best efficiency ζ_{st} is achieved with particle sizes of 10–20 mm. However, if much longer standby periods are necessary, larger particles may be more advantageous.

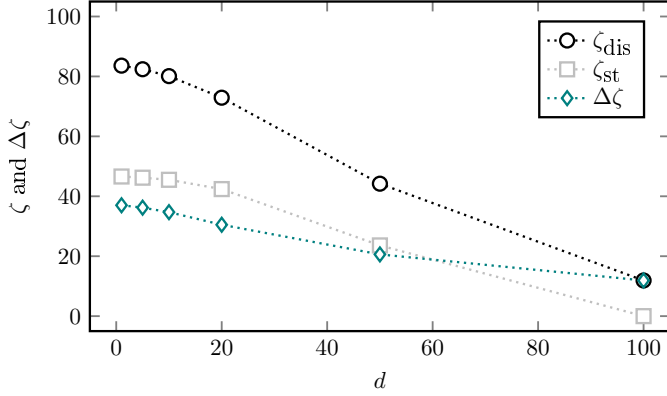


Figure 10: Thermocline efficiency after discharge ζ_{dis} (in %) and after an additional standby ζ_{st} (in %) depending on the particle size d (in mm)

4.2.2. Variation of the thermal conductivity λ_s

The smallest thermocline regions in the fluid and thus, the most efficient discharge process, can be seen in Fig. 11 for the highest thermal conductivity of the particles. This is also indicated by the intra-particle temperature difference in Fig. 12, which is minimum due to the excellent heat transfer in highly thermally conductive filler material. The maximum intra-particle temperature difference for $\lambda_s = 50$ W/mK is $\Delta T_{p,\text{max}} = 1$ K, compared with $\Delta T_{p,\text{max}} = 149$ K for $\lambda_s = 0.1$ W/mK.

As shown in Fig. 13, a high thermal conductivity leads to the best results during discharge ($\zeta_{\text{dis}} = 52.2\%$ for $\lambda_s = 50$ W/mK), as the heat transfer is improved. However, the increase of the thermocline efficiency is negligible for $\lambda_s > 10$ W/mK. Indeed, above this value, the convective heat transfer resistance between the filler material and the surrounding fluid dominates, thus preventing further improvement of ζ_{dis} as λ_s increases.

On the contrary, during standby, thermal conductivity values lower than 1 W/mK considerably reduce the expansion of the thermocline, because of the prevailing conductive thermal resistance in the filler material over the filler-fluid convective one. This is shown by the decreasing values of the thermocline growth $\Delta\zeta$ in Fig. 13 (according to Eq. 16). Thus, the optimum thermal conductivity of the filler material for the reference case of this study is $\lambda_s \approx 5\text{--}10$ W/mK, but is, of course, depending on the standby time.

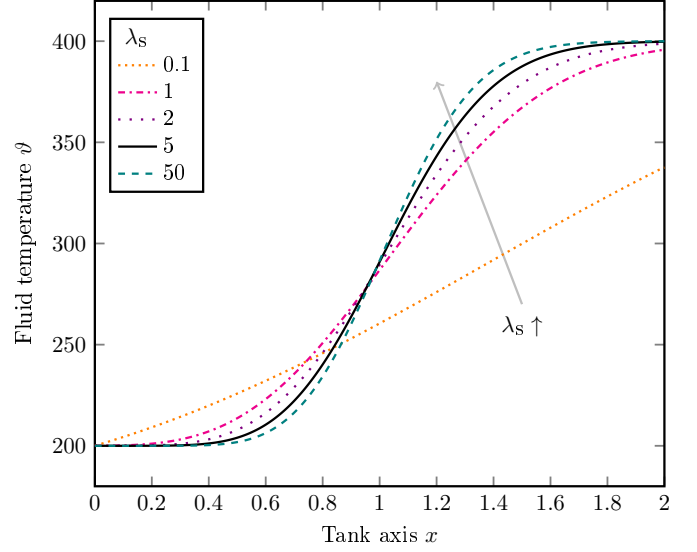


Figure 11: Fluid temperature ϑ (in $^{\circ}\text{C}$) along the vertical tank axis x (in m) after discharge (t_{dis}) depending on the thermal conductivity of the filler λ_s (in W/mK)

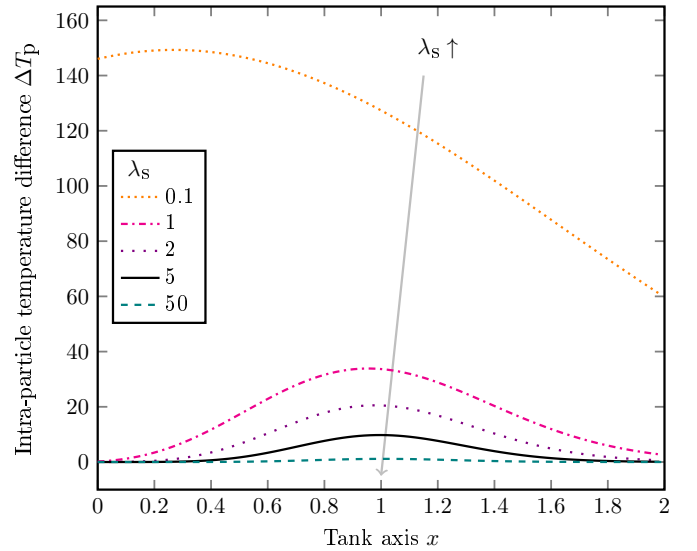


Figure 12: Intra-particle temperature difference ΔT_p (in K) along the vertical tank axis x (in m) after discharge (t_{dis}) depending on the thermal conductivity of the filler λ_s (in W/mK)

4.2.3. Variation of the volumetric heat capacity $(\rho c_p)_s$

The influence of the volumetric heat capacity on the fluid and filler material temperatures in the storage tank during discharge is presented in Fig. 14 and Fig. 15. The temperature profile along the vertical axis is steeper for low values of $(\rho c_p)_s$ resulting in lower thermocline thicknesses and therefore higher efficiencies.

The same positive effect is found in the intra-particle temperature decrease with decreasing $(\rho c_p)_s$. For $(\rho c_p)_s = 5 \cdot 10^7$ kJ/(m^3K) the maximum intra-particle temperature difference is $\Delta T_{p,\text{max}} = 10$ K, for $(\rho c_p)_s = 5 \cdot 10^5$ kJ/(m^3K) it is $\Delta T_{p,\text{max}} = 8$ K.

Nevertheless, the volumetric heat capacity has a reduced

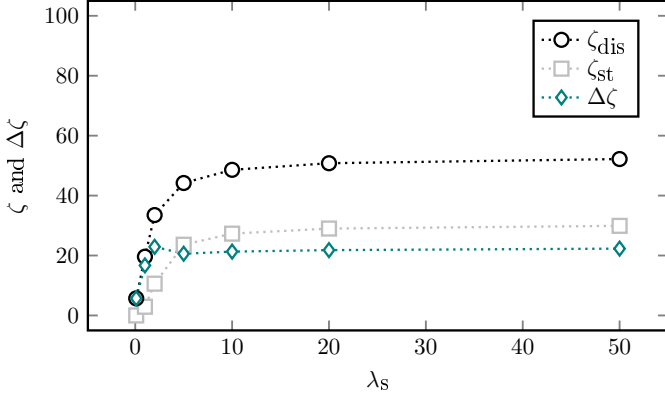


Figure 13: Thermocline efficiency after discharge ζ_{dis} (in %) and after an additional standby ζ_{st} (in %) depending on the thermal conductivity of the filler λ_s (in W/mK)

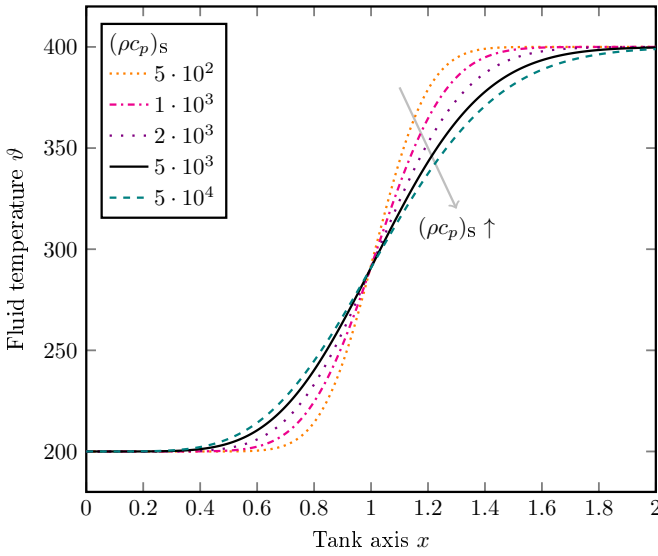


Figure 14: Fluid temperature ϑ (in °C) along the vertical tank axis x (in m) after discharge (t_{dis}) depending on the volumetric heat capacity $(\rho c_p)_s$ (in kJ/(m³K))

influence on the discharge compared with the diameter and thermal conductivity, as can be observed by the small changes the fluid temperature in Fig. 14 and the intra-particle temperature difference in Fig. 15. This is due to the simultaneous reduction of the discharge time with lower $(\rho c_p)_s$ (Table 4).

As shown in Fig. 16, although low values of $(\rho c_p)_s$ increase the thermocline efficiency during discharge, high values favour the standby operation. The reason is a decreased thermal diffusivity in the filler particles ($\lambda_s/(\rho c_p)_s$) which reduces the heat diffusion processes inside them. For the standby time of this study, high values of $(\rho c_p)_s$ even lead to an overall increase of the combined discharge and standby operation. Moreover, it is beneficial from an economic point of view to store the main part of the heat in (low-cost) filler material with a high volumetric heat capacity [17].

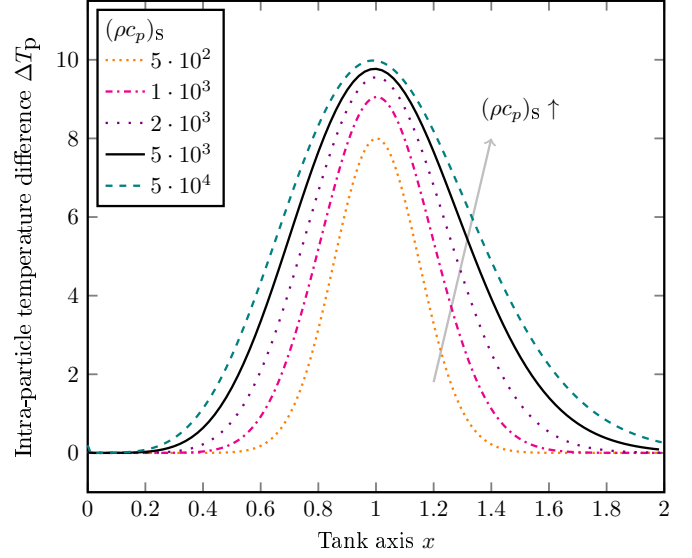


Figure 15: Intra-particle temperature difference ΔT_p (in K) along the vertical tank axis x (in m) after discharge (t_{dis}) depending on the volumetric heat capacity $(\rho c_p)_s$ (in kJ/(m³K))

Table 4: Filler mass, storage capacity and discharge time for varied volumetric heat capacities of the filler

$(\rho c_p)_s$ kJ/(m ³ K)	m_s kg	Q kWh	t_{dis} min
$5 \cdot 10^2$	251.9	27.4	12
$1 \cdot 10^3$	356.3	37.3	16
$2 \cdot 10^3$	503.8	57.1	24
$5 \cdot 10^3$	796.6	116.5	49
$1 \cdot 10^4$	1126.6	215.4	91
$5 \cdot 10^4$	2519.1	1007.1	426

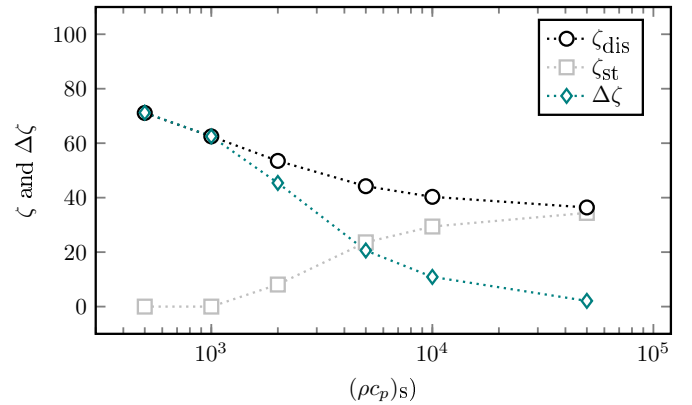


Figure 16: Thermocline efficiency after discharge ζ_{dis} (in %) and after an additional standby ζ_{st} (in %) depending on the volumetric heat capacity $(\rho c_p)_s$ (in kJ/(m³K))

4.2.4. Main effects and interactions of the parameters

In order to assess the magnitude of the effects of the influencing parameters and their interactions on the result, a full factorial DOE was performed. The results of the cases described in Table 3 are summarized in Table 5 with

the target value y_i being either the thermocline efficiency ζ or the thermocline growth during standby $\Delta\zeta$. Efficiency values of zero imply that the thermocline region fills the entire tank (Eq. 12).

The three parameters A, B and C correspond to the filler particle diameter d , the thermal conductivity λ_s , and the volumetric heat capacity of the filler $(\rho c_p)_s$, respectively. The correlations between these parameters are given by the combinations of A, B and C.

The effects of these parameters, which are presented in Fig. 17–19 are calculated according to Eq. 17. The results are shown in Fig. 17 for the discharge, in Fig. 18 for the combined discharge and standby and in Fig. 19 for the thermocline growth $\Delta\zeta$.

Table 5: Results for y_i after t_{dis} and additional standby of 480 min (8h) for the 2^k tests according to Table 3

	y_1	y_2	y_3	y_4
ζ_{dis}	82.7%	26.7%	82.8%	58.4%
ζ_{st}	0%	0%	0%	0%
$\Delta\zeta$	88.7%	26.7%	82.8%	58.4%
	y_5	y_6	y_7	y_8
ζ_{dis}	83.2%	6.9%	83.9%	12.9%
ζ_{st}	76.0%	0%	76.4%	6.3%
$\Delta\zeta$	7.2%	6.9%	7.5%	6.6%

It can be concluded from Fig. 17 that increasing the diameter of the filler (A) has a strongly negative effect on ζ_{dis} . An increase of the volumetric heat capacity (C) leads to a decrease of ζ_{dis} as well, whereas a larger thermal conductivity (B) has a positive effect on the thermocline efficiency. However, the effects of B and C and the interdependencies between the parameters are rather limited, in comparison with the effect of A.

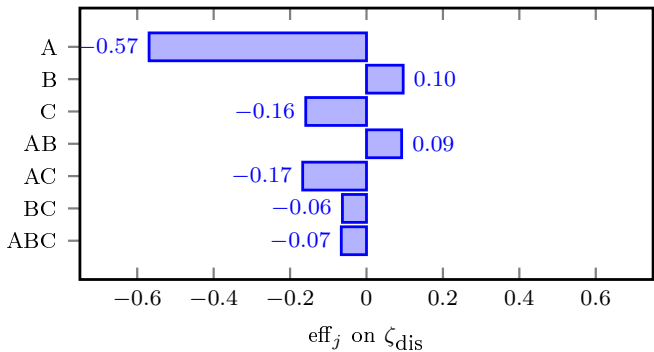


Figure 17: Magnitude of effects and interactions of the factors A ($\hat{=} d$), B ($\hat{=} \lambda_s$) and C ($\hat{=} (\rho c_p)_s$) on ζ_{dis}

Considering the combined discharge and standby (Fig. 18), the increase in volumetric heat capacity (C) results in an increased thermocline efficiency ζ_{st} , comparable to its decrease due to larger filler diameters (A). The negative value of the interaction AC indicates that a simultaneous increase in filler diameter (A) reduces the effect of increasing

the volumetric heat capacity (C) on ζ_{st} , but promotes the negative effect of factor A.

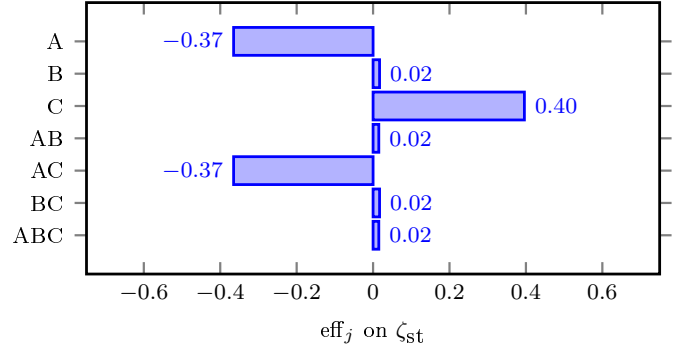


Figure 18: Magnitude of effects and interactions of the factors A ($\hat{=} d$), B ($\hat{=} \lambda_s$) and C ($\hat{=} (\rho c_p)_s$) on ζ_{st}

The results shown in Fig. 19 indicate that the dominating parameter on the thermocline growth is the volumetric heat capacity (C). The negative value of C results in a reduced growth of the thermocline region during standby as $(\rho c_p)_s$ increases. The filler diameter (A) has an approximately 3 times smaller and also negative influence on $\Delta\zeta$, leading to a reduced growth of the thermocline during standby with larger particles. If both filler diameter (A) and volumetric heat capacity (C) are increased simultaneously (interaction AC) it leads to a reduced effect of both factors. The influence of the thermal conductivity (B) and the interdependencies AB, BC and ABC can be neglected in comparison. It should be noted, that in the numerical model point contact between the filler particle spheres is assumed and thus, no inter-particle heat conduction is considered.

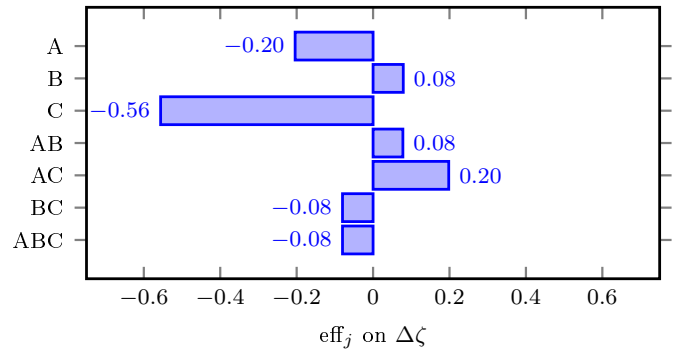


Figure 19: Magnitude of effects and interactions of the factors A ($\hat{=} d$), B ($\hat{=} \lambda_s$) and C ($\hat{=} (\rho c_p)_s$) on $\Delta\zeta$

5. Conclusion

In this work a dual-media storage system composed of a liquid metal (lead-bismuth eutectic) and a filler material is numerically analysed. The geometry and operating conditions correspond to those of a 100-kWh pilot-scale

storage system currently under construction at the Karlsruhe Institute of Technology with a tank height of 2 m and a diameter of 0.6 m in order to select the optimum filler material and size for the experiment. To the best of the authors' knowledge, it will be the first-of-its-kind dual-media storage system with liquid metal as heat transfer fluid.

The general conclusions, however, can be transferred to any liquid metal dual-media storage system. The simulations are carried out for the discharge phase and the combined discharge and standby operation. The thermocline efficiency is evaluated and compared for different values of the filler diameter d , the thermal conductivity λ_s and the volumetric heat capacity $(\rho c_p)_s$ by varying one factor at a time and by using a full factorial design of experiment.

- d : The discharge phase is favoured by small diameter particles, however with no significant improvement for very small sizes (for the reference case chosen in this work: $d < 10$ mm). During standby, by contrast, larger particles are preferred. The combination of the two shows an optimum for diameters of about 10–20 mm for the considered reference case.
- λ_s : The thermal conductivity also has opposing effects on the discharge and standby phases. The former is favoured by high values while the latter by low ones. For the reference case in this study, a value of 5–10 W/mK represents an excellent compromise between the two.
- $(\rho c_p)_s$: A low volumetric heat capacity improves the thermocline efficiency during the discharge phase, as the storage volume is kept constant as well as the fluid mass flow leading to shorter discharge times, which improve the thermocline behaviour significantly. A high volumetric heat capacity, however, favors the standby phase. Moreover, due to the relatively high cost of liquid metals it is preferable to store energy in cheap fillers with high volumetric heat capacity.
- The combined effects of the parameters on the thermocline efficiency are analysed through a full factorial analysis. It shows that the filler diameter has the strongest effect on the thermocline efficiency during the discharge phase. For the combined discharge and standby phase, the filler material and the volumetric heat capacity prevail, with opposite effects on the thermocline efficiency. When only the standby phase is considered, the volumetric heat capacity dominates. According to this analysis, the effect of the thermal conductivity does not have a dominating influence on the results.
- Studies in the literature with molten salt or thermal oil show that small filler diameters and a high thermal conductivity (in case of large particles) are beneficial for the discharge process. However, these studies do not consider a parametric analysis of the filler size and properties during standby. As the thermal conductivity of molten salt and thermal oil is

significantly lower than that of the liquid metal, the selection of the filler material does not seem to be as relevant as for the liquid-metal based storage system. For the latter, the standby is especially challenging and thus, the filler material needs to buffer the thermocline degradation with a low thermal conductivity, opposite to conventional heat transfer fluids.

Nomenclature

Subscripts

dis	Discharge
f	Fluid
i	Inner
max	Maximum
min	Minimum
o	Outer
p	Particle
th	Thermocline
s	Solid
st	Standby
v	Volumetric

Acronyms

DOE	Design of experiments
KIT	Karlsruhe Institute of Technology
LBE	Lead-bismuth eutectic

Latin letters

A	factor in DOE
B	factor in DOE
C	factor in DOE
c_p	Specific heat capacity ($\text{Jkg}^{-1}\text{K}^{-1}$)
d	Filler particle diameter (mm)
D	Tank diameter (m)
eff_j	Effects in full factorial DOE (-)
H	Tank height (m)
h_v	Volumetric heat transfer coefficient ($\text{Wm}^{-3}\text{K}^{-1}$)
m	Mass (kg)
\dot{m}	Mass flow (kgs^{-1})
Q	Storage capacity (J)
s_v	Specific surface (m^{-1})
t	Time (s)
T	Fluid temperature (K)
T_p	Particle temperature (K)
u	Fluid velocity in packed bed (ms^{-1})
Δx_{th}	Thermocline thickness (m)
x	Coordinate along tank height (m)
y	Coordinate along particle radius (m)
y_i	Test result in full factorial DOE (-)

Greek letters

α	Heat transfer coefficient ($\text{Wm}^{-2}\text{K}^{-1}$)
$\Delta\zeta$	Thermocline growth during standby (%)
ε	Bed porosity (-)
ϑ	Fluid temperature ($^{\circ}\text{C}$)
ζ	Thermocline efficiency (%)
λ	Thermal conductivity ($\text{Wm}^{-1}\text{K}^{-1}$)
ρ	Density (kgm^{-3})

References

- [1] M. Mehos, H. Prince, R. Cable, D. Kearney, B. Kelly, G. Kolb, F. Morse, Concentrating Solar Power Best Practices Study, Technical Report NREL/TP-5500-75763, Golden, CO: National Renewable Energy Laboratory (NREL), 2020.
- [2] T. Bauer, C. Odenthal, A. Bonk, Molten salt storage for power generation, *Chemie Ingenieur Technik* 93 (2021) 534–546.
- [3] J. Edwards, H. Bindra, P. Sabharwal, Exergy analysis of thermal energy storage options with nuclear power plants, *Annals of Nuclear Energy* 96 (2016) 104–111.
- [4] C. Forsberg, Separating nuclear reactors from the power block with heat storage to improve economics with dispatchable heat and electricity, *Nuclear Technology* 0 (2021) 1–23.
- [5] J. Coventry, C. Andraka, J. Pye, M. Blanco, J. Fisher, A review of sodium receiver technologies for central receiver solar power plants, *Solar Energy* 122 (2015) 749–762.
- [6] J. Pacio, A. Fritsch, C. Singer, R. Uhlig, Liquid metals as efficient coolants for high-intensity point-focus receivers implications to the design and performance of next-generation CSP systems, *Energy Procedia* 49 (2014) 647 – 655. Proceedings of the SolarPACES 2013 International Conference.
- [7] H. Bommelburg, C. Smith, Sodium-NaK engineering handbook, Chapter 1 Physical Properties, Gordon & Breach, New York, 1976.
- [8] OECD-NEA, Handbook on Lead-bismuth Eutectic Alloy and Lead Properties, Materials Compatibility, Thermal-hydraulics and Technologies, OECD/NEA Nuclear Science Committee Working Party on Scientific Issues of the Fuel Cycle Working Group on Lead-bismuth Eutectic, 2007.
- [9] A. Fritsch, C. Frantz, R. Uhlig, Techno-economic analysis of solar thermal power plants using liquid sodium as heat transfer fluid, *Solar Energy* 177 (2019) 155–162.
- [10] S. Polimeni, M. Binotti, L. Moretti, G. Manzolini, Comparison of sodium and KCl-MgCl₂ as heat transfer fluids in CSP solar tower with sCO₂ power cycles, *Solar Energy* 162 (2018) 510–524.
- [11] J. Pacio, T. Wetzel, Assessment of liquid metal technology status and research paths for their use as efficient heat transfer fluids in solar central receiver systems, *Solar Energy* 93 (2013) 11 – 22.
- [12] G. Wang, T. Wang, W. Han, Cyclic and standby behavior evaluations of liquid lead-bismuth eutectic thermal energy storage tank for concentrated solar power, *Case Studies in Thermal Engineering* 29 (2022) 101729.
- [13] I. D. Piazza, A. Tincani, R. Marinari, M. Valdiserri, S. Bassini, A. Rinaldi, M. Serra, A. Antonelli, D. Delfino, Conceptual design of the CSP lead demonstrator SOLEAD, *Advanced Materials Letters* 11 (2020) 1–7.
- [14] A. Palacios, C. Barreneche, M. Navarro, Y. Ding, Thermal energy storage technologies for concentrated solar power – a review from a materials perspective, *Renewable Energy* 156 (2020) 1244–1265.
- [15] B. D. Pomeroy, Thermal energy storage in a packed bed of iron spheres with liquid sodium coolant, *Solar Energy* 23 (1979) 513–515.
- [16] K. Niedermeier, J. Flesch, L. Marocco, T. Wetzel, Assessment of thermal energy storage options in a sodium-based CSP plant, *Applied Thermal Engineering* 107 (2016) 386–397.
- [17] K. Niedermeier, L. Marocco, J. Flesch, G. Mohan, J. Coventry, T. Wetzel, Performance of molten sodium vs. molten salts in a packed bed thermal energy storage, *Applied Thermal Engineering* 141 (2018) 368–377.
- [18] K. Niedermeier, Numerical investigation of a thermal storage system using sodium as heat transfer fluid (PhD thesis, KIT Scientific Publishing, KIT-SR 7755) (2019).
- [19] T. Laube, L. Marocco, K. Niedermeier, J. Pacio, T. Wetzel, Thermodynamic analysis of high-temperature energy storage concepts based on liquid metal technology, *Energy Technology* 8 (2019) 1900908.
- [20] C. Xu, X. Li, Z. Wang, Y. He, F. Bai, Effects of solid particle properties on the thermal performance of a packed-bed molten-salt thermocline thermal storage system, *Applied Thermal Engineering* 57 (2013) 69–80.
- [21] M. Cascetta, G. Cau, P. Puddu, F. Serra, Numerical investigation of a packed bed thermal energy storage system with different heat transfer fluids, *Energy Procedia* 45 (2014) 598–607.
- [22] Z. Yang, S. V. Garimella, Cyclic operation of molten-salt thermal energy storage in thermoclines for solar power plants, *Applied Energy* 103 (2013) 256–265.
- [23] J. T. Van Lew, P. Li, C. L. Chan, W. Karaki, J. Stephens, Analysis of heat storage and delivery of a thermocline tank having solid filler material, *J. Sol. Energy Eng.* 133 (2011) 021003.
- [24] J.-F. Hoffmann, T. Fasquelle, V. Goetz, X. Py, A thermocline thermal energy storage system with filler materials for concentrated solar power plants: Experimental data and numerical model sensitivity to different experimental tank scales, *Applied Thermal Engineering* 100 (2016) 753–761.
- [25] K. Reddy, V. Jawahar, S. Sivakumar, T. Mallick, Performance investigation of single-tank thermocline storage systems for CSP plants, *Solar Energy* 144 (2017) 740–749.
- [26] E. Votyakov, A. Bonanos, Algebraic model for thermocline thermal storage tank with filler material, *Solar Energy* 122 (2015) 1154–1157.
- [27] V. Palomba, A. Frazzica, Application of numerical methods for the design of thermocline thermal energy storage: Literature review and critical analysis, *Journal of Energy Storage* 46 (2022) 103875.
- [28] P. J. Roache, Perspective: A method for uniform reporting of grid refinement studies, *Journal of Fluids Engineering* 116 (1994) 405–413.
- [29] J. Almendros-Ibáñez, M. Fernández-Torrijos, M. Díaz-Heras, J. Belmonte, C. Sobrino, A review of solar thermal energy storage in beds of particles: Packed and fluidized beds, *Solar Energy* 192 (2019) 193–237.
- [30] M. Morris, *Design of Experiments - An Introduction Based on Linear Models*, CRC Press, Boca Raton, Fla, 2011.
- [31] P. D. Berger, R. E. Maurer, G. B. Celli, *Experimental Design*, Springer International Publishing, 2018.